Scattering States for Very Low Energy Electron Spectroscopy

C. Solterbeck, O. Tiedje, F. Starrost, and W. Schattke
Institut für Theoretische Physik, Christian-Albrechts-Universität Kiel, Leibnizstraße 15, D-24098 Kiel, Germany

A recently developed method for treating scattering states is further investigated and extended. It yields the wave functions as used e.g. in a calculation for electron diffraction at very low energies or for photoemission in the one-step model at vacuum-ultraviolet photon frequencies. The necessity of non-muffin tin potentials at these energies for covalent bond solids is obvious. The method uses a Laue representation as well as the full direct space applying also multigrid techniques.
Keywords: Photoemission, VLEED, Scattering States

I. INTRODUCTION

Solution for the scattering states of the half crystal using the Schrödinger equation and the Lippman-Schwinger equation are presented with both, the discretization in full direct space and the Laue representation. The usual approach which is vastly exploited for structure determinations by low energy electron diffraction (LEED) consists in a multiscattering procedure based on an angular momentum representation. The extension beyond the muffin-tin assumption to a full potential including the surface barrier potential suffers from slow convergence of the angular momentum expansion for low energies. The opposite approach uses the so called Laue representation with plane waves in the surface parallel directions, and the direct space along the surface perpendicular (z-) axis. In both methods, the application to large unit cells soon meets the boundaries of computer ressources. However, many of the current ab-initio electronic and surface structure calculations use a plane wave basis, and it is desirable to close up to those procedures for the scattering states of the conduction bands as well. Thus the adequate procedure seems still to be in question for a full potential calculation which is indispensable especially for the low energy states of photoemission.

In comparison with the huge literature on multiscattering related to LEED investigations, plane wave and direct space based treatments are rare and suffered in the past from instabilities introduced by connecting the crystal wave function with the vacuum by means of a propagator. The origin of these difficulties could be traced back to the formulation as an initial value problem. A solution to those problems offers the quantum transmitting boundary method (QTBM)[1] which replaced matching by a mathematically well defined boundary value problem. Such an approach has been applied by Joly in full direct space.[2] For a formulation in the Laue representation we tested various solvers for the discretized algebraic system. It became apparent that a multigrid procedure with respect to the third, i.e. surface perpendicular, dimension was competitive to direct algebraic solvers.[3]

A further possibility to transform the initial value problem into a boundary value problem consists in the use of Green's functions which adequately describe the asymptotic behavior in infinite distance. If one takes the solutions for a rectangular step at the solid-vacuum interface and constant optical potential inside the solid, the Green's function in the Laue representation can be obtained analytically. The kernel of the Lippman-Schwinger integral then contains the residual potential, i.e. the periodic one inside the solid and the interface corrugation potential, and, of course, the Green's function.

There is one drawback with classical algebraic methods applied to the Lippman-Schwinger equation or to the Schrödinger equation. The amount of 100 reciprocal surface lattice vectors and a mesh of 1000 points in z-direction seems to be rather modest, but lies at the limit of standard computers. Furthermore, the calculation of one final state takes on a CRAY CPU about 1000 seconds using the simple matching algorithm and 100 seconds using a multigrid routine in the Laue representation. For a full hemisphere photoemission calculation c. 1500 final states are needed at least.[4,5] The initial state calculation and that of the matrix elements consumes negligible time on that scale. Consequently, a strong demand exists for a fast algorithm.

Since multigrid algorithms have proven to be highly successful in classical fields it is worth to test these algorithms also in the cases considered here, especially in a full direct space treatment of the Schrödinger case. If the linear scaling of multigrid methods can prove to be more efficient in any of these problems, then it should at least become apparent in an application taking into account all three dimensions. First applications of multigrid techniques to the Bloch states of the bandstructure have shown to be successful.[6]

Besides the above reasons for these investigations an explicit knowledge of the wavefunction bears additional advantages. It simplifies the calculation and it offers a direct illustration of the photoemission final state which may be used for the interpretation of the transition and of the emission spectra. So we present in the following several of the studied methods and focus on the shape of the wavefunction and its consequences for the distribution of the photoemitted electrons.

II. GREEN'S FUNCTION APPROACH

In this section the Laue representation is used. The Schrödinger equation for a general local potential reads

$$\left(\partial_z^2 + \mathbf{k}_f^2 - (\mathbf{k}_\parallel + \mathbf{g})^2 - \frac{2m}{\hbar^2} V_{opt}(z)\right) \alpha_{k_\parallel+g}(z) = \frac{2m}{\hbar^2} \sum_{g'} v_{g-g'}(z) \alpha_{k_\parallel+g'}(z) \quad (1)$$

with the wave function $\psi_{k_\parallel}(z,\boldsymbol{\rho}) = \sum_g \alpha_{k_\parallel+g}(z) e^{i(\mathbf{k}_\parallel+\mathbf{g})\boldsymbol{\rho}}$. Here, $\mathbf{k}_f$ denotes the wavevector of the escaping electron, $\mathbf{k}_\parallel$ the surface parallel Bloch vector, and $\boldsymbol{\rho}$ the two-dimensional position vector. In order to transform to an integral equation with the correct asymptotic behavior the Green's function is chosen in a simple manner, just solving for each reciprocal surface lattice vector $\mathbf{g}$ a onedimensional step potential along the z-axis with the suitable boundary values.

$$\left.\begin{array}{l} \left(\partial_z^2 + \kappa_g^2(z)\right) G(z,z';\mathbf{g}) = \delta(z-z'), \\ \kappa_g^2(z) = \mathbf{k}_f^2 - (\mathbf{k}_\parallel + \mathbf{g})^2 - \frac{2m}{\hbar^2} V_{opt}(z) \end{array}\right\} \quad (2)$$

The optical potential V_{opt} recently was obtained via the selfenergy on an ab-initio basis for the bulk.[4] The step function part of a generalized halfspace V_{opt} defines the z-dependence of $\kappa_g^2(z)$ with the asymptotic value $k(\kappa)$ for $z \to +\infty(-\infty)$. This way the halfspace problem is properly reproduced. The final equation

$$\alpha_{k_\parallel+g}(z) = f_g(z) + \frac{2m}{\hbar^2} \sum_{g'} \int_{-\infty}^{+\infty} dz' G(z,z';\mathbf{g}) v_{g-g'}(z') \alpha_{k\parallel+g'}(z') \quad (3)$$

uses a homogenous solution of Eq. 2 for $f_g(z) = \delta_{k_{f\parallel},k_\parallel+g} f_0(z) (\propto e^{ik_{f\perp}z}, z \to \infty)$. The solution for Green's function can be written as

$$\begin{aligned} G(z,z';\mathbf{g}) = & \\ & -\tfrac{1}{i(k+\kappa)} \exp(-i\kappa(z)|z| - i\kappa(z')|z'|) * \\ & \left(\left|\tfrac{\kappa(z)-\kappa(z')}{k-\kappa}\right| + 1 - \tfrac{k+\kappa}{\kappa(z)+\kappa(z')}\right) \\ & + i \exp(-\tfrac{i}{2}(\kappa(z)+\kappa(z'))|z-z'|) * \\ & \left|\tfrac{1}{k-\kappa} - \tfrac{k+\kappa}{(k-\kappa)(\kappa(z)+\kappa(z'))}\right| \end{aligned} \quad (4)$$

dropping the index $\mathbf{g}$.

A Picard iteration into a Born series has proven to converge only for a sufficiently small periodic potential as could be expected from general arguments. However, this equation is appropriate also for algebraic solvers. The system is characterized by a matrix factorizing into two, one being Green's matrix with dimension given by the z-discretization and diagonal in the reciprocal surface lattice vectors. The other is given by the potential which has a shape depending on the considered potential and on the discretization , e.g. for a local potential in the Laue representation the matrix is band diagonal. Apart from the Born series, the capabilities of this formulation were tested by applying a conjugate gradient procedure (BiCG) for an iterative solution. A Nyström discretization of the integral in full direct space would lead to a sparse potential matrix and thus ease the application of multigrid methods.

III. SCHRÖDINGER EQUATION WITH QTBM

The Schrödinger equation is written in direct space and the boundary condition reads

$$\begin{aligned} & \partial_z \psi(\boldsymbol{\rho}, z_{max}) = \\ & \sum_g i\kappa_g e^{i(\mathbf{k}_\parallel+\mathbf{g})\boldsymbol{\rho}} \Big(2\delta_{g,0} e^{i\kappa_\mathbf{g} z_{max}} - \\ & \tfrac{1}{\mu(\Omega_1)} \int_{\Omega_1} e^{-i(\mathbf{k}_\parallel+\mathbf{g})\boldsymbol{\rho}'} \psi(\boldsymbol{\rho}', z_{max}) d\boldsymbol{\rho}'\Big) \end{aligned} \quad (5)$$

with $\kappa_\mathbf{g} = -\sqrt{\frac{2m}{\hbar^2}(E - \Phi_{th}) - (\mathbf{k}_\parallel + \mathbf{g})^2}$ and threshold Φ_{th}. This equation results from the QTBM conditions as described[1,3] and z_{max} denotes an arbitrary value far in vacuum. Because the right hand side is constant around z_{max}, this equation may be integrated to get rid of the z-derivative. At $z = 0$, the boundary deep in the solid, the wave function is set equal to zero owing to the optical potential. Bloch conditions are required for the boundaries in the surface parallel planes. One transforms to coordinates parallel to the lattice vectors $\mathbf{a}_1$ and $\mathbf{a}_2$ within the plane by the matrix $(\phi_{11}, \phi_{12}, \phi_{21}, \phi_{22}) = (1, -\cot\alpha, 0, 1)$. Here, α denotes the angle between the lattice vectors, $a = |\mathbf{a}_1|$ and $b = |\mathbf{a}_2| \sin(\alpha)$. One obtains for the periodic part u of the wavefunction

$$\begin{aligned} -\tfrac{\hbar^2}{2m} & \big[(\tfrac{1}{\sin^2\alpha})\partial_1^2 u + \partial_2^2 u + \partial_z^2 u - 2\cot\alpha\, \partial_1\partial_2 u \\ & + 2i(k_1 - k_2\cot\alpha)\partial_1 u + 2ik_2\partial_2 u\big] \\ & + (V - E - V_{opt} + \tfrac{\hbar^2}{2m}{\mathbf{k}_\parallel}^2) u = 0 \end{aligned} \quad (6)$$

$$\left.\begin{array}{rcl} u(x_1+a, x_2, z) &=& u(x_1,x_2,z), \\ u(x_1, x_2+b, z) &=& u(x_1,x_2,z), \\ u(x_1,x_2,0) &=& 0 \end{array}\right\} \quad (7)$$

$$u(\boldsymbol{\rho}, z) = f(z) + \sum_g e^{i\kappa_\mathbf{g}(z-z_{max})} e^{i\mathbf{g}\boldsymbol{\rho}} \tfrac{1}{ab} \int u(\boldsymbol{\rho}', z_{max}) e^{-i\mathbf{g}\boldsymbol{\rho}'} d\boldsymbol{\rho}' \quad (8)$$

with $f(z) = 2i\sin(\kappa_0(z - z_{max})) e^{i\kappa_0 z_{max}}$. Defining

$$\alpha_{l,j} = \sum_{\mu=0}^{N_1-1} \sum_{\nu=0}^{N_2-1} e^{i\kappa_{\mu,\nu}(z-z_{max})} e^{-2\pi i(\frac{l\mu}{N_1} + \frac{j\nu}{N_2})} \quad (9)$$

the last equation reads

$$f(z_{max} - h_z) = u_{i,j,N_3-1} - \frac{h_1 h_2}{ab} \sum_{j'=1}^{N_2} \sum_{i'=1}^{N_1} u_{i',j',N_3} \alpha_{i-i'(\mathrm{mod}N_1),j-j'(\mathrm{mod}N_2)} \quad (10)$$

After discretizing the Laplacian the final system is written in matrix form as $L\underline{u} = \underline{f}$. The matrix L is band diagonal with matrices A_i on the diagonal and $\frac{1}{h_z^2}\mathbf{1}$ on the sub- and supradiagonal. Exceptionally, in the lower right-hand corner there is the matrix of the QTBM, V. A blocking according to the three cartesian indices is applied. The equation containing the block matrix V derives from Eq. 10. Apart from the band diagonal terms cyclic terms at the corners of the matrix arise from the inplane periodic boundary conditions. In comparison with the Lippman-Schwinger equation, the resulting matrix is sparse besides the QTBM block. The latter complicates the numerics in this case whereas for the former case the dense Green's matrix increases the computational amount.

The multigrid technique uses the interchange of a direct solution on a coarse-grained grid with an iterative refinement on a fine grid. It exploits the smoothing properties of the latter and replaces its bad convergence for the low Fourier components by an exact solution for the correction on the large scale grid. In this investigation several direct solvers and several iteration procedures were tested.

IV. RESULTS

The methods are not formally restricted to special properties of potentials. However, singular potentials will be difficult to be treated, both with the Laue representation because of high wave vector components and with the direct space representation because of dense grids. At present, pseudopotentials seem to be the most suitable. The normconserving nonlocal ab-initio potentials[7] as well as their localization[8–10] are well adapted for the direct space methods. For the nonlocal potential an averaging procedure over the angles has to be applied.[11] The localized version can also easily be combined with the Laue representation, as the Fourier transform to the bulk reciprocal lattice is done mostly analytically[10] and the backtransform to the z-dependence, i.e. the surface perpendicular direction, needs only a small set of fast one-dimensional Fourier transforms. Best suited for testing and estimating the quality of the different solution schemes are the semiempirical pseudopotentials[12] because of their simple handling.

Fig. 1 shows a final state for photoemission in the vacuum ultraviolet (VUV) photon regime for normal and strongly inclined emission. It has been calculated with the Green's function method for the case of an ideal Si(001) surface. The integral equation has been algebraically solved with a BiCG algorithm. There is a significant variation of the escape depth, i.e. the length scale in z-direction over which the wave function is different from zero. It varies with incidence direction and less pronounced also with energy. It is known and explained by a path length's argument that electron spectroscopy at inclined angles probes especially the surface properties. Here, this effect becomes quantum mechanically directly visible. It shows how the empirical escape depth curve which describes the energy dependence is subject to the variation of the angle. The normal emission plot, on one hand, gives an impression how deep the wavefunction penetrates into the solid and thus makes it possible to detect bulk properties like dispersion in normal emission spectra. On the other hand, full hemisphere photoemission patterns show in the outer regions the electronic structure of an extremely thin surface slice. Additionally, an energy and angle dependent fine structure is observed which is correlated with the atomic positions.

In Fig. 2 the charge density of an outgoing state in normal emission is plotted as obtained from a multigrid calculation for the perpendicular component of the Laue representation.[3] To illustrate the high nonspherical contributions at that energy the potential is displayed in one inset. The initial state charge density in a second inset gives an idea of what can be expected from a photoemission calculation. The matrix element for that transition roughly consists of an integral over two factors each going monotonically with one of both charge densities. If one neglects the phases, volumes with large initial and final state charges should contribute more significantly. The observed strong local dependence of the final state can lead to a characterization of emissions as arising from specific orbitals and sites of the initial state.

The change in the phase distribution of the final state is shown in Fig. 3 by varying the emission direction and excitation energy. The surfaces of constant phase are seen to be normal to the escape direction. Especially in normal emission, the flat and constant shape of these surfaces through all layers is obvious. It impressively demonstrates the phase coherence and thus the strict $\mathbf{k}_{\parallel}$- and relaxed $k_{\perp}$-momentum conservation. This stresses again the dominance of bulk transitions in normal emission. Also for inclined emission angles this phase coherence is observed, though it is of less importance in the deeper layers because of the vanishing modulus. The perturbation of the coherence is confined to the surface-near space which is the main emitting region for inclined angles and which, therefore, influences appreciably the photocurrent.

In summarizing the foregoing discussion, besides the fundamental quantum mechanical properties which are nicely seen in the wavefunctions many details arise. Already a qualitative look at the charges and phases allows an understanding of common experience. The detailed properties, only briefly sketched here, could be systematically analyzed to get a more direct picture of photoemission. The feasibility of both presented formalisms for numerical calculations could be proved, and a further optimization in speed and memory within the developed frame will be attainable.

This work was supported by the "Bundesministerium für Bildung, Wissenschaft, Forschung und Technologie" (Project No. 05 605 FKA).

[1] C. S. Lent and D. J. Kirkner, J. Appl. Phys. **67**, 6353 (1990).

[2] Y. Joly, Phys. Rev. Lett. **68**, 950 (1992); Phys. Rev. B **53**,13 029 (1996).

[3] S. Lorenz, C. Solterbeck, W. Schattke, J. Burmeister, W. Hackbusch, Phys. Rev. B **55**, R13432 (1997).

[4] W. Schattke, Prog. Surf. Sci. **54**, 211 (1997).

[5] C.-H. Solterbeck, W. Schattke, C.S. Fadley, Surf. Sci. **357-358**, 245 (1996).

[6] E.L. Briggs, D.J. Sullivan, and J. Bernholc, Phys. Rev. B **54**, 14362 (1996).

[7] D.R. Hamann, M. Schlüter, and C. Chiang, Phys. Rev. Lett. **43**, 1494 (1997).

[8] G.B. Bachelet, D.M. Ceperley, and M.G.B. Chiocchetti, Phys. Rev. Lett. **62**, 2088 (1989).

[9] W.M.C. Foulkes and M. Schlüter, Phys. Rev. B **42**, 11505 (1990).

[10] A. Bödicker, W. Schattke, Phys. Rev. B **55**, 5545 (1997).

[11] J.R. Chelikowski, N. Troullier, K. Wu, and Y. Saad, Phys. Rev. B **50**, 11355 (1994).

[12] M.L. Cohen and T.K. Bergstresser, Phys. Rev. **141**, 789 (1966).

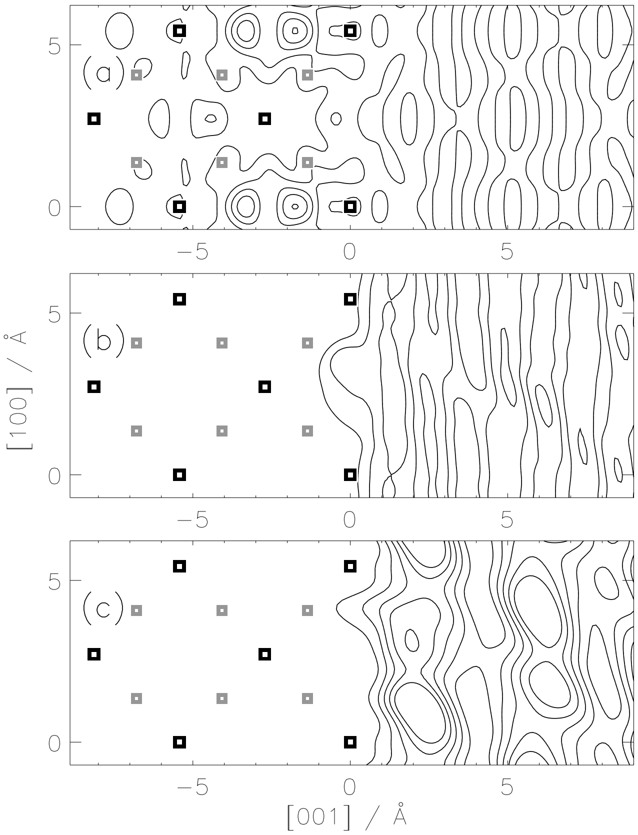

FIG. 1. Contour plots of the Si charge density in the plane of the [100] and [001] directions. The atoms lying in the plane are drawn black and the projected positions of the remaining atoms are grey. The contour levels are the same for all plots. Three different combinations of the emission angle and the final state energy are shown: (a) E_{fin} = 55 eV for normal emission; (b) E_{fin} as before but for a polar angle of 70° and the azimuth in the shown plane; (c) angles as before, but with E_{fin} = 21 eV.

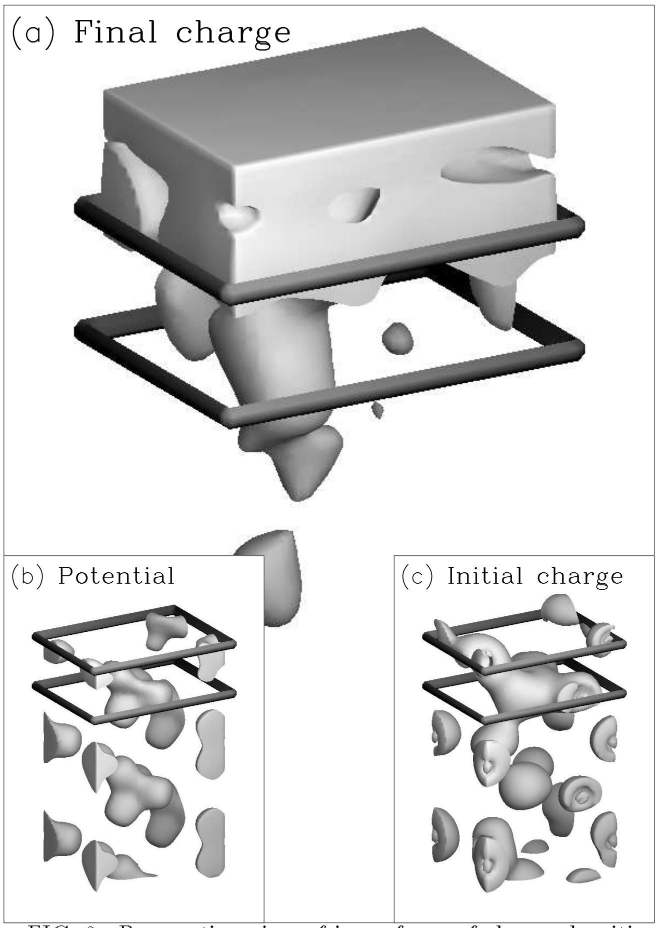

FIG. 2. Perspective view of isosurfaces of charge densities and potential of the GaAs(110) surface. A surface unit cell is shown with As atoms at the corners in the uppermost plane. The surface perpendicular range extending from 0.35 a in the vacuum at the top of the images to -1.7 a inside the bulk. (a) Charge density of a scattering state with $\mathrm{E}_{fin} = 17$ eV, $\vartheta = 19.4°$, and $\phi = 195°$; (b) Potential at an energy level at which the smaller values around the Ga sites are not visible; (c) Charge density of a bound state at $\mathrm{E}_{ini} =$ -4 eV and a $\mathbf{k}_{\|}$ belonging in a photoemission process to the final state of (a). As a guide to the eye frames are added indicating the positions of the uppermost two atomic layers.

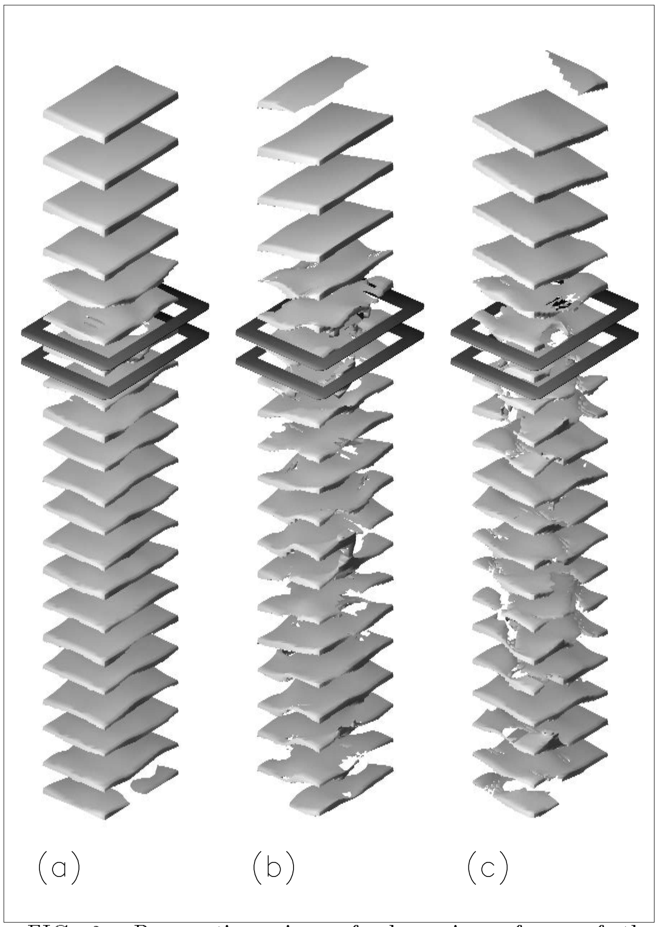

FIG. 3. Perspective view of phase isosurfaces of the GaAs(110) surface. Three different combinations of the emission angle and the final state energy are shown: (a) $\mathrm{E}_{fin} =$ 18 eV for normal emission; (b) $\mathrm{E}_{fin} = 18$ eV, $\vartheta = 17.62°$, $\phi = 180°$; (c) $\mathrm{E}_{fin} = 20$ eV, $\vartheta = 17.62°$, $\phi = 55°$. A unit cell in the surface parallel directions with As atoms at the corners is shown. The surface perpendicular range extends over 3 lattice constants into the vacuum at the top of the images and to 6 lattice constants into the bulk. The additional frames indicate the position of the uppermost two atomic layers.